Urban Rail Transit (2024) 10:13–27
https://doi.org/10.1007/s40864-023-00209-x

http://www.urt.cn/

ORIGINAL RESEARCH PAPERS

Research on Vibration Characteristics of a Flexible Vehicle-Ladder Track System

Huan Wang[1] · Aijun Gu[2] · Qiang Fan[3] · Xing Xing[4] · Jingyu Liu[5]

Received: 6 August 2023 / Revised: 9 November 2023 / Accepted: 10 November 2023 / Published online: 19 January 2024

Abstract As a means of vibration reduction, the ladder track has seen broad implementation in urban rail transit. However, issues such as increased vibration noise, rail corrugation, and fastener failure have been observed in certain sections of the ladder track during later operation. To investigate the mechanisms behind these phenomena and provide comprehensive insights into the system's response to various operational conditions, this study employed vehicle-track coupled dynamic theory to establish a three-dimensional finite element model of the flexible vehicle-ladder track system. The vibration transmission and dynamic response characteristics of the vehicle-ladder track system were analyzed. The findings revealed that the vehicle-track resonance and anti-resonance phenomena were more prominent in the medium- to low-frequency range. At specific frequencies, the wheelset exhibited various vibration modes, and the fastener force was found to closely correlate with the ladder vibration mode. Furthermore, the influence of speed on diverse components of the vehicle-ladder track system, in terms of maximum vibration and the dominant vibration frequency range, differed considerably. This study provides a more comprehensive and reasonable exploration of the modeling and dynamic behavior of vehicle-ladder track systems.

Keywords Ladder track · Vehicle-track coupled dynamics · Vibration transmission characteristics · Vibration mode · Dynamic response

1 Introduction

Urban rail transit is one of the largest public infrastructure projects in many cities, and will have profound impacts on urban development and the lives of citizens. In China, as of May 2023, a total of 54 cities in 31 provincial-level regions and the Xinjiang Production and Construction Corps have opened 292 urban rail transit lines, with an operating mileage of 9652.6 km. However, the issue of vibration caused by urban rail transit has become increasingly serious. Therefore, various vibration reduction measures have been used to protect sensitive areas along the lines from vibration impacts. Among them, the floating ladder track, developed by the Railway Technical Research Institute (RTRI) in Japan, has been widely applied in urban rail transit systems in recent years, such as the Nankai Main Line, the Airport Line between Izumisano and Rinku Town Stations, Beijing Subway Line 5, Shanghai Subway Line 2, and others [1, 2]. The ladder track consists of rails, fasteners, ladder-shaped sleepers, resilient pads, and a concrete track bed. Additionally, the ladder sleeper is designed as a ladder configuration, comprising twin longitudinal prestressed concrete beams which are rigidly connected to transverse steel-pipe connectors. Multiple theoretical analyses and engineering applications have demonstrated that the ladder track effectively

✉ Jingyu Liu
cars-liujy@qq.com

[1] School of Highway, Chang'an University, Xi'an 710064, China

[2] School of Civil Engineering, Beijing Jiaotong University, Beijing 100044, China

[3] China Construction South Investment Co., Ltd, Shenzhen 441000, China

[4] Beijing General Municipal Engineering Design and Research Institute Co., Ltd., Beijing 100082, China

[5] Railway Engineering Research Institute, China Academy of Railway Sciences Corporation Limited, Beijing 100081, China

Communicated by Liang Gao.

mitigates vibration and noise [3–5]. However, during later operation, it has been observed that although the ladder track provides certain isolation effects, issues such as increased vibration noise, rail corrugation, and fastener failure become prominent in certain sections [6–9].

The vibration of the vehicle–track interaction plays a crucial role in the occurrence of rail corrugation [10]. In order to elucidate the relationship between rail corrugation generation and vibration in the ladder track, researchers have conducted a series of in-depth studies. Xiao et al. [11] investigated the correlation between the occurrence of rail corrugation and vibration in the ladder track through field observations and numerical simulations obtained from the vehicle-track rigid-flexible coupling model. Li et al. [12] found that rail corrugation was related to the intrinsic vibration properties of the ladder track system considering partial elasticity and the train's speed for different radius curves. Li et al. [13] conducted research on a 350-m curved ladder-type sleeper track, combining field measurements and numerical modeling. Their investigation highlighted the significant role played by lateral bending vibrations of the rail relative to the ladder-type sleepers in the development of rail corrugation. Fan et al. [14] established a rigid vehicle-flexible ladder sleeper track model to investigate vehicle dynamic performance and stability index in both tangent and curved track sections. It is worth noting that, despite their comprehensive nature, these studies either did not fully account for the coupling between the track and vehicle or addressed partial flexibility in the coupling.

Existing research has also focused on specific aspects related to vibration mitigation in the ladder track in terms of numerical and experimental methods. Jin et al. [15] compared the effects of three different layouts of resilient pads under the sleeper on the dynamic characteristics of the ladder track using a multi-input multi-output modal testing method. Yan et al. [16] examined the influences of fastening parameters and resilient pad parameters on the vibration in the ladder track using a vehicle track-coupled numerical model. Wang et al. [17] suggested a device in the ladder track to mitigate vibration and improve train operation stability. Optimization was achieved by governing the primary frequency range of rail vibration, the rail vibration amplitude, and the total power transmitted to the foundation, aiming to reduce the vibration issues caused by the ladder track [16, 18–20]. Despite these advancements, a comprehensive analysis of the ladder track's systematic vibration transmission and dynamic response characteristics, including the influence of speed on system components and the correlation between fastener force and vibration modes, remains relatively limited.

Additionally, some researchers have undertaken qualitative investigations into ladder track dynamics and key parameters under varying load conditions using analytical methods. For example, Mohammadzadeh et al. [21] examined the dynamic response of a ladder track subjected to periodic moving loads, employing an infinitely long Timoshenko beam on a random elastic foundation. Roger et al. [1] explored the free and forced vibration characteristics of ladder track using a Bernoulli–Euler beam with infinite length under moving loads. While these qualitative studies have offered valuable insights, they have been limited in capturing the complex dynamic behavior of vehicle ladder track systems.

Consequently, this study seeks to establish a three-dimensional flexible finite element (FE) model of the coupled vehicle-ladder track system and both conducting systematic vibration transmission characteristics and dynamic response characteristics of the vehicle-ladder track system. This examination could also assist in tackling practical concerns, including insights into the system's response to various operational conditions and the implementation of vibration control measures.

2 Numerical Model

2.1 Three-Dimensional Coupled Dynamic FE Model of the Vehicle-Ladder Track

The initial step involved conducting a frequency analysis to examine the vibration transmission characteristics. This analysis was performed using the FE wheelset-ladder track model. Subsequently, the wheelset-ladder track model was expanded to create a more comprehensive vehicle-ladder track model.

Since this study primarily focused on the vertical vibration behavior of the wheelset and track, the impact of motor position on vertical vibration was found to be negligible [22]. Therefore, no motor was installed on the wheelset. The LM wear-type tread was employed in accordance with the Chinese standard GB449-2016 [23]. The wheelset model was assumed to be elastic, isotropic, and homogeneous, and it was modeled using solid elements. The constraints of the primary suspensions were also indicated, as depicted in Fig. 1. To determine the wheelset's vertical vibration receptance, a unit force Fz was applied to the wheels at the wheel-rail contact points A and B. Following that, the resulting vertical vibrations of the wheelset were calculated.

The ladder track model consisted of a pair of rails, fasteners, ladder sleepers, and resilient pads. It was once again assumed to be elastic, isotropic, and homogeneous. In the FE modeling, the rails and steel-pipe connectors were represented by Timoshenko beam elements, while the fasteners and resilient pads were modeled using spring-damper elements. The sleepers were simulated using solid elements, as illustrated in Fig. 2. In a similar manner, the receptance

function of the ladder track could be determined by applying a unit force at point A′, denoted as Fz', in the opposite direction to Fz. The vertical vibrations of the track were then calculated. To couple the ladder track model and wheelset model, the vehicle-track contact was simplified as a linear relationship to facilitate calculations, and the contact stiffness was set to 4.4 GN/m.

This flexible vehicle-ladder track model was expanded from the wheelset-ladder track model and included a single wagon system consisting of four wheelsets, two bogies, and a car body, as illustrated in Fig. 3. It incorporated a primary suspension responsible for connecting the wheelsets to the bogie frame and a secondary suspension that coupled the bogie frame to the car body. The bogie and car body shared the same characteristics of being elastic, isotropic, and homogeneous, and they were both modeled using solid elements. In contrast, the primary and secondary suspensions were represented by spring-damper elements.

Detailed parameters for both the B-type metro train and ladder track can be found in Tables 1 and 2, respectively. For the purpose of comparative analysis, a vehicle-conventional monolithic track coupling FE model was also established. The vehicle parameters and track component parameters were kept the same as those of the ladder track, while the only differentiation lies in the track structure.

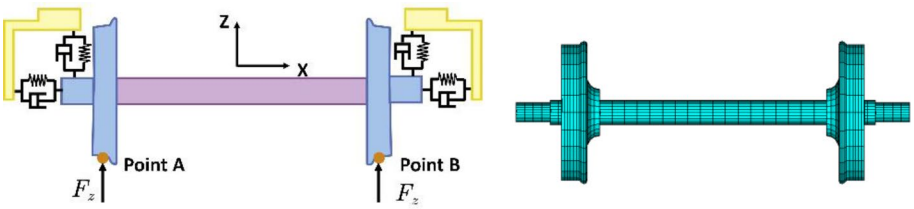

Fig. 1 The FE wheelset model

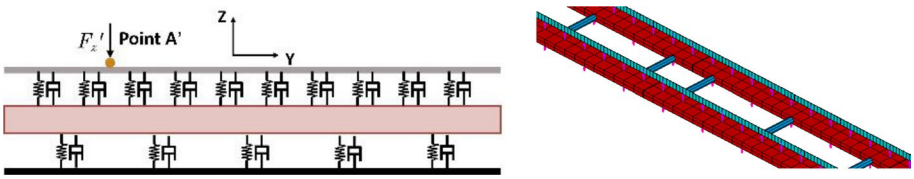

Fig. 2 The FE ladder track model

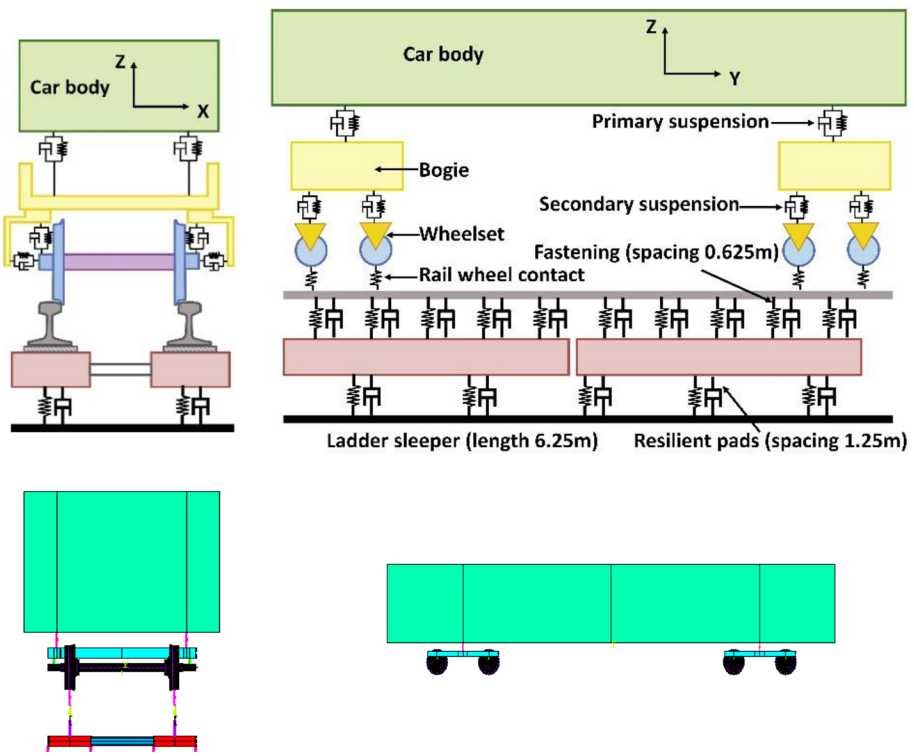

Fig. 3 The flexible vehicle-ladder track model

Table 1 Parameters of B-type metro train

Category	Parameter	Value (unit)
Inertia parameters	Vehicle body mass	21,920 kg
	Axle weight	140 kN
	Wheelset mass	1420 kg
	Bogie frame mass	2550 kg
Geometry parameters	Vehicle dimensions L×W×H	19 m×2.8 m×3.8 m
	Bogie wheelbase	2.2 m
	Vehicle bogie spacing	12.6 m
	Lateral spacing of primary suspension (prim. susp.)	1.93 m
	Lateral spacing of secondary suspension (sec. susp.)	1.85 m
	Wheel diameter	0.84 m
Suspension parameters	Vertical stiffness of the prim. susp.	1.7 MN/m
	Lateral stiffness of the prim. susp.	10.4 MN/m
	Vertical stiffness of the sec. susp.	0.275 MN/m
	Lateral stiffness of the sec. susp.	0.3 MN/m
	Vertical damping of the prim. susp.	5 kN·s/m
	Vertical damping of the sec. susp.	30 kN·s/m
	Lateral damping of the sec. susp.	30 kN·s/m
Material parameters	Elastic modulus of the wheel and axle	206 GPa
	Poisson's ratio of the wheel and axle	0.257
	Elastic modulus of the vehicle body and bogie	206 GPa
	Poisson's ratio of the vehicle body and bogie	0.3

Table 2 Parameters of ladder track

Parameters		Value (unit)
Rail	Rail type	60 kg/m
	Elastic modulus	210 GPa
	Poisson's ratio	0.3
Fastener	Stiffness	45 MN/m
	Damping	10 kN s/m
	Interval	0.6 m
Sleeper	Elastic modulus	35 GPa
	Density	2500 kg/m^3
	Poisson's ratio	0.17
Resilient pad	Stiffness	25 MN/m
	Damping	10 kN s/m
	Interval	1.2 m

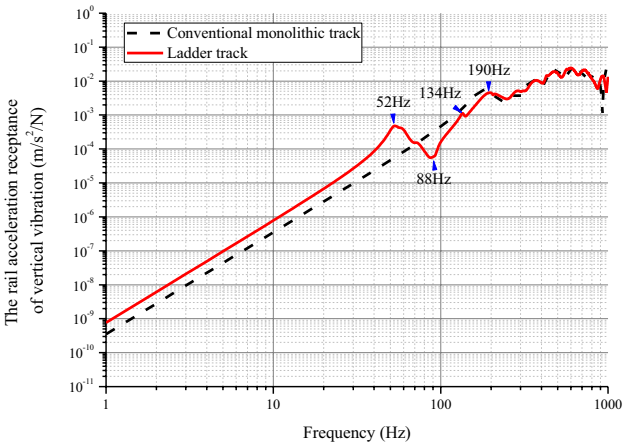

Fig. 4 Vertical vibration receptance of rail

2.2 Model Validation

To validate the model, the vibration acceleration transfer function of the rail was obtained numerically as shown in Fig. 4. It can be observed that the ladder track primarily affects the vibration characteristics of the rail within the frequency range of 0–200 Hz. Peaks in vibration occur at frequencies of 52 Hz, 134 Hz, and 190 Hz. In order to exclude the effect of other factors on the rail vibration, a comparison was made between the ladder track and the conventional monolithic track; see also in Fig. 4. One can observe that the vibration at 52 Hz and 134 Hz is solely induced by the ladder track.

Fig. 5 presents the results of the impact hammer test conducted on the ladder track at the experimental platform of Beijing Jiaotong University. The test utilized a Dytran 5802A force hammer, ZonicBook/618E data acquisition system, LC0123 accelerometer (for the rail), and LC0108 accelerometer (for the ladder sleeper). It can be observed that the frequency response function reaches a peak at 134 Hz. In reference [13], field measurements and tests were conducted on the rail corrugation of a subway ladder

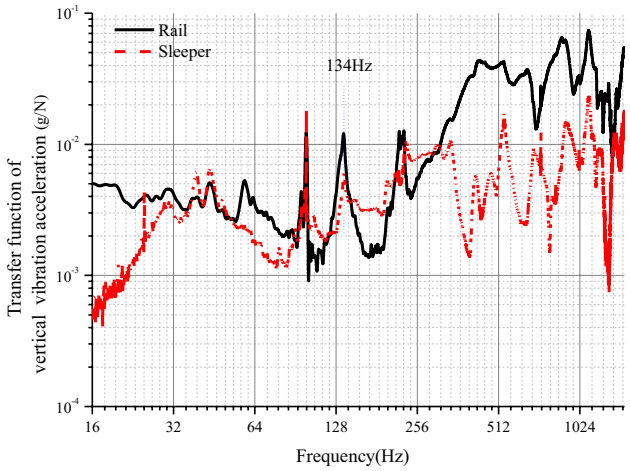

Fig. 5 Frequency–response function of the ladder track

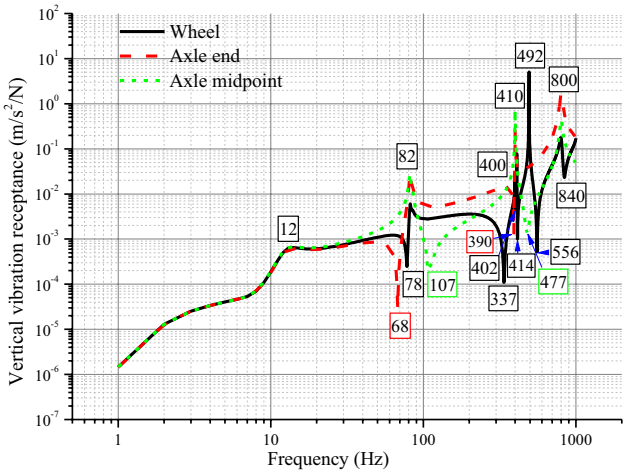

Fig. 6 The vertical vibration receptance of the wheelset

track. Based on the measured wavelength and train speed, the frequency of the rail corrugation was calculated to be 138 Hz. The rail and sleeper displayed peak accelerations around 134 Hz and 132 Hz, respectively, as revealed by power spectral density measurements.

The numerical results including both frequency analysis and time-domain analysis indicate that the dominant resonant frequency of the track is approximately 134 Hz, which agrees well with the results obtained from the experiment platform and field measurements of the ladder track. Therefore, the comparison between the numerical simulation results and experimental data demonstrates the reliability and accuracy of the proposed model in capturing the dynamic response and vibration properties of the ladder track.

3 Vertical Vibration Transmission Characteristics of the Vehicle-Track Coupled System

To acquire an understanding of the vibrational responses of different wheelset-track components within the dominant frequency range and the propagation of vibrations, an analysis of vibration transmission characteristics in the frequency domain was conducted. This analysis could also aid in addressing some practical issues, such as the mechanisms behind rail corrugation generation, fastening failures at specific frequencies, and vibration control within a specific frequency range. Initially, the vertical vibration transmission characteristics were analyzed for the wheelset and ladder track individually. Subsequently, the vibration transmission characteristics of the vehicle-track coupled system were analyzed by introducing contact forces.

3.1 Analysis of Vertical Vibration Transmission Characteristics in the Wheelset

An analysis was conducted on the vibration transfer properties of the wheelset within the frequency range of 0–1000 Hz, and the vibration acceleration transfer function was obtained, as shown in Fig. 6.

It can be noted that minimal disparity exists in the vertical vibration of the wheel and the axle within the frequency range of 0–50 Hz. The wheel exhibits vibration peaks at 12 Hz, 82 Hz, 410 Hz, 492 Hz, and 800 Hz, while vibration valleys occur at 78 Hz, 337 Hz, 414 Hz, 556 Hz, and 840 Hz. Both the axle end and axle midpoint exhibit vibration peaks at 12 Hz, 82 Hz, 400 Hz, and 800 Hz, with the axle end showing vibration valleys at 68 Hz, 390 Hz, and the axle midpoint showing valleys at 107 Hz and 477 Hz. From Fig. 6, it can be observed that there are six consecutive resonant frequencies and six consecutive anti-resonant frequencies exhibited by the wheel across the frequency band of 0 to 1000 Hz, while the axle exhibits fewer resonances and anti-resonances compared to the wheel. The vibration modes of the wheelset at resonance and anti-resonance frequencies were analyzed in detail, as shown in Figs. 7 and 8. In these and subsequent figures, the gray grid represents the undeformed configuration.

According to Fig. 7, the vibration modes of the wheelset at 12 Hz and 82 Hz are similar to those of a rigid body, where no elastic deformation occurs and only vertical motion takes place. At 400 Hz, the wheelset exhibits a specific vibration mode defined as M-mode. In this mode, the axle midpoint vibrates downwards, while the axle ends vibrate upwards. Simultaneously, the bottom of the wheel experiences lateral inward vibration, while the upper part of the wheel undergoes minimal vibration deformation. At 410 Hz, the wheelset undergoes minimal vertical vibration deformation

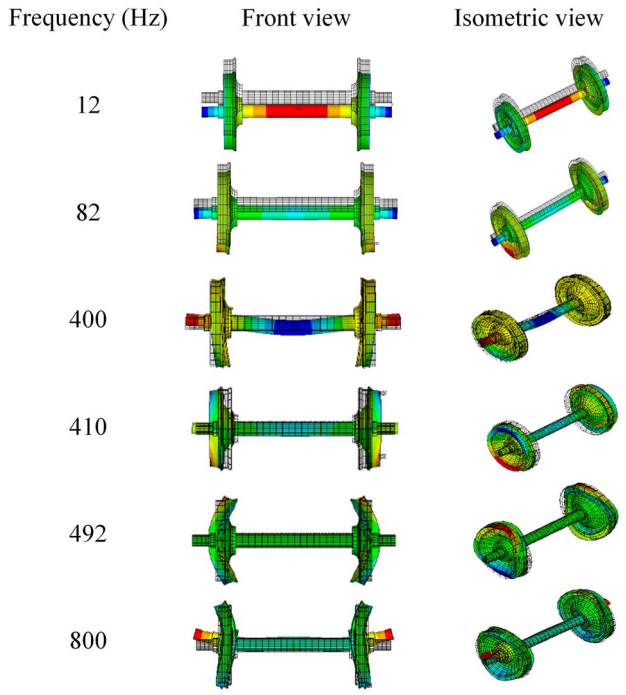

Fig. 7 Vibration mode of the wheelset system under the resonant frequency

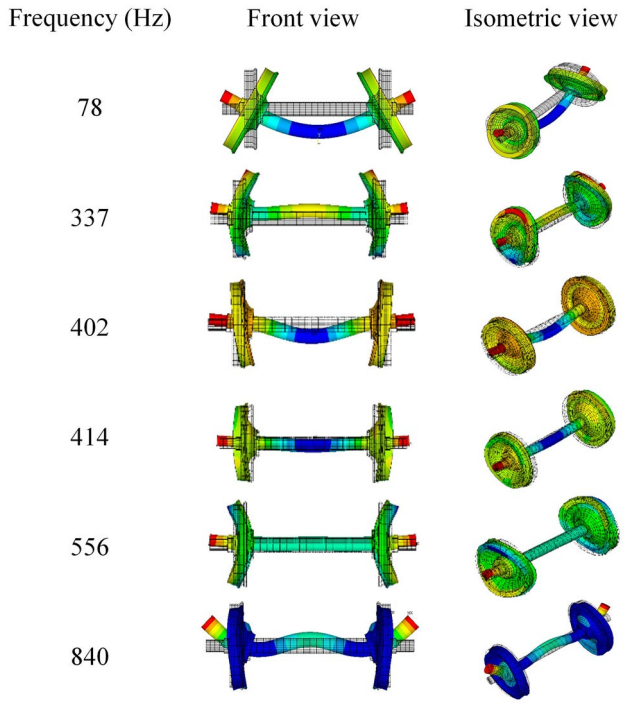

Fig. 8 Vibration mode of the wheelset system under the anti-resonant frequency

but experiences transverse stretching and shrinking vibrations. At 492 Hz, the axle of the wheelset undergoes minimal vibration deformation, while the wheel bends vertically. At 800 Hz, both axle midpoint and axle end vibrate either upwards or downwards, with the vibration amplitude being greater at the axle end compared to that of the axle midpoint, where the bottom and part of the wheel experiences lateral outward vibration, while the middle vibrates inwards.

According to Fig. 8, the vibration modes of the wheelset at anti-resonance frequencies were analyzed as follows:

At 78 Hz, the axle undergoes vertical bending vibration, and the wheel remains perpendicular to the axle throughout. At 337 Hz, both the axle ends and midpoint vibrate either upwards or downwards with similar amplitudes. The wheel undergoes bending vibration, with the vibration amplitude at the top of the wheel being larger than that at the bottom, And the alignment between the axle and the wheel deviates from perpendicular. At 402 Hz, the wheelset exhibits M-mode vibration, with the axle midpoint vibrating downwards, the axle ends vibrating upwards, and the bottom part of the wheel vibrating laterally towards the axle midpoint, while the wheel top experiences smaller vibrations relative to the bottom. At 414 Hz, the entire wheelset undergoes transverse stretching and shrinking vibration, and only the middle section of the axle undergoes minor vertical vibrations. At 556 Hz, the middle section of the axle undergoes minimal vibration deformation, axle ends vibrate upwards, and the wheel undergoes vertical bending vibration, with little difference in vibration amplitude between the upper and lower parts of the wheel. At 840 Hz, the vibration mode, known as W-mode vibration, is characterized by both the axle ends and the middle portion of the axle vibrating upwards, with the wheel demonstrating a lower vibration amplitude compared to the axle.

3.2 Analysis of Vertical Vibration Transmission Characteristics in the Ladder Track

In 2.2, it was observed that the ladder track exhibited vibration peaks at frequencies of 52 Hz, 88 Hz, and 134 Hz. Therefore, an analysis of the vibration modes at these frequencies was conducted and compared with the conventional monolithic track, as shown in Fig. 9. Overall, the two track structures differ significantly at frequencies around 52 Hz, 88 Hz, 134 Hz, and 190 Hz. However, the distinctions in vibration modes between the two tracks become less prominent beyond the resonance frequency of 190 Hz. Therefore, it can be concluded that the impact of the ladder track on the vertical rail vibration is primarily concentrated within the frequency range of approximately 0–200 Hz. As demonstrated in this study through field measurements or platform experiments, it has been consistently observed that the third-order resonance frequency 134 Hz is the main factor

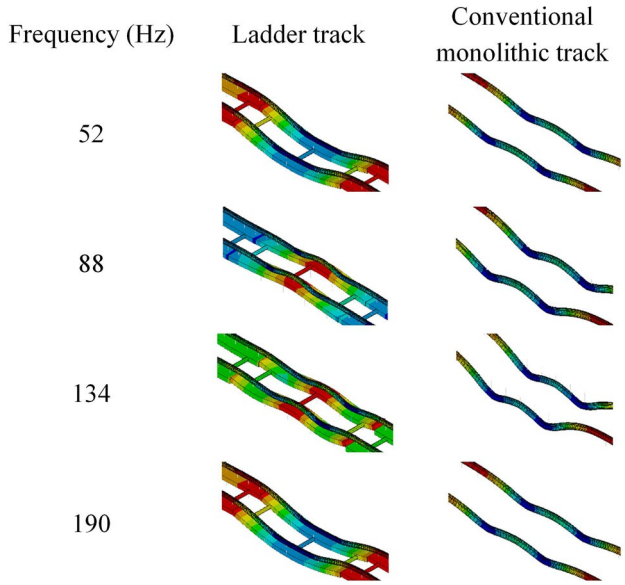

Fig. 9 Vibration mode of track under different frequencies

leading to rail corrugation. Therefore, to mitigate corrugation problems induced by this vibration, appropriate optimization metrics, such as the primary frequency range of rail vibration, can be chosen for further optimization analysis.

3.3 Analysis of Vertical Vibration Transmission Characteristics in the Coupled Vehicle-Ladder Track System

In addition to analyzing the individual vibration characteristics of the wheelset and the track, this study also investigated the vertical vibration transmission characteristics of the vehicle-ladder track system. By coupling the track and the vehicle together, contact springs were employed and excitation at the vehicle-track contact points was applied, and the vibration responses at different frequencies were computed. The vertical vibration transmission characteristics are shown in Fig. 10.

Figure 10 reveals that the vehicle-track system exhibits consecutive six resonance frequencies (40 Hz, 78 Hz, 112 Hz, 404 Hz, 488 Hz, 756 Hz) and four anti-resonance frequencies (110 Hz, 320 Hz, 340 Hz, 518 Hz) within the range of 0–1000 Hz. The vibration modes at the resonance and anti-resonance frequencies of the vehicle-track system are shown in Figs. 10 and 11, respectively.

From Fig. 11, it can be observed that at 40 Hz, the wheel, axle, rail, and sleeper undergo the first resonance frequency. The vibration mode is characterized by downward bending of the axle, synchronized vibration of the wheel with the rail and sleeper in the same direction, and the wheel maintaining its vertical position without significant deformation. At 78 Hz, the vibration of the rail and sleeper is significantly

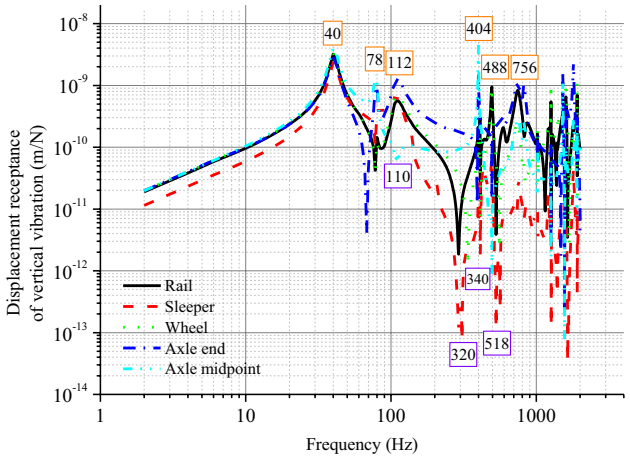

Fig. 10 The displacement receptance of the vertical vibration of the vehicle-track system

smaller than that of the wheelset. The axle and track vibrate in the same direction, while the wheel vibrates in the opposite direction relative to the track, with the wheel remaining vertical to the axle. At 112 Hz, the vibration characteristics of the rail and sleeper differ between the two wheelsets. The sleeper under one wheelset exhibits the opposite vibration direction compared to the vehicle-track system, while the sleeper under the other wheelset exhibits the same vibration direction. In other words, different wheelsets and track sections exhibit different vibrations. At 404 Hz, the vibration

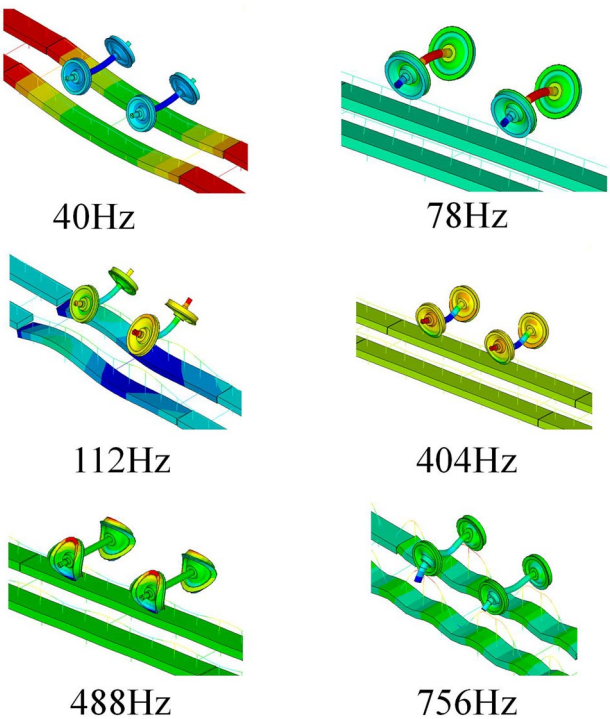

Fig. 11 Vibration mode of track/wheel at resonant frequencies

primarily occurs in the wheelset system, with minimal vibration in the track system. The middle portion of the axle undergoes downward bending vibration, with the vibration amplitude at the axle ends being smaller. The contact portion of the wheel with the rail experiences slight vibration. At 488 Hz, the axle does not vibrate significantly, while the wheel undergoes bending vibration and the rail exhibits noticeable vertical vibration. At 756 Hz, the axle ends and midpoint undergo downward vibration, and resonance occurs between the lower wheel and the track system, while the rail and sleeper between the two wheelsets experience resonance. Resonance frequencies in either the wheelset or the rail should be avoided during the design phase to prevent exacerbated vibration and noise issues, which can be highly destructive to urban rail transit systems.

According to Fig. 12, at 110 Hz, the vibrations of the two wheelsets are similar, but the vibration characteristics of the track differ. The rail and sleeper under the wheelset with a larger vibration amplitude exhibit anti-resonance, while those under the wheelset with a smaller amplitude exhibit resonance. The axle undergoes vertical bending vibration. At 320 Hz, the wheel begins to undergo bending vibration, and the middle section of the axle and axle end simultaneously undergo downward or upward vibration. The wheel and the track system experience anti-resonance, while the vibration of the sleeper is relatively small. At 340 Hz, the vibration mode of the wheelset is similar to that at 320 Hz. The wheel resonates with the rail while exhibiting anti-resonance with the sleeper. At 518 Hz, the axle midpoint undergoes minimal vibration, while the axle ends undergo slight upward vibration. The wheel undergoes bending vibration and resonates with the rail while exhibiting anti-resonance with the sleeper.

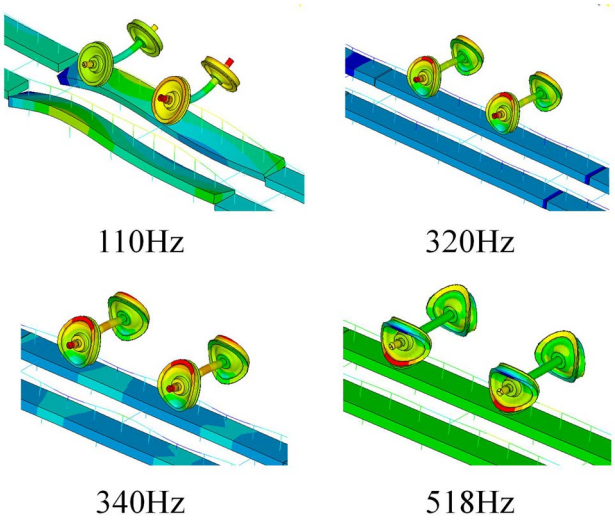

Fig. 12 Vibration mode of track/wheel at anti-resonant frequencies

The vibration modes at the vibration peaks are generally considered to represent typical vibrations within a frequency range; therefore, the vibration modes at different frequency ranges are depicted in Fig. 13 to gain a detailed understanding of the typical vibration behavior.

In the frequency range of 70–78 Hz, the wheelset undergoes bending vibration while remaining perpendicular to the axle. The vibration trend of the rail and ladder sleeper is consistent, but opposite to that of the wheel. In the frequency range of 78–170 Hz, the wheel and rail exhibit similar vibration modes. The vibration trend of the ladder sleeper and rail

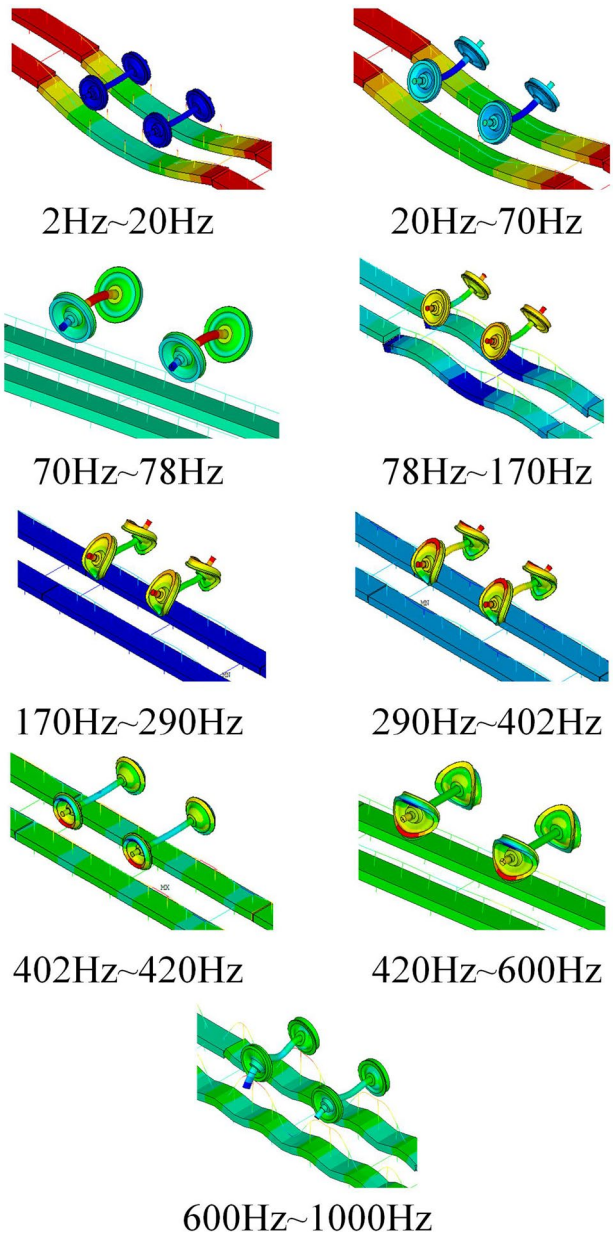

Fig. 13 Vibration mode of the wheel and track of the vehicle-track coupling system under particular frequencies

is opposite for the right-side wheelset, while it is consistent for the left-side wheelset. Between the frequencies of 290–402 Hz, the vibration behavior of the ladder sleeper shows an inverse relationship to that of the rail, albeit with smaller amplitude. The wheel and rail also exhibit opposite vibration trends. At the peak of the rail vibration, a hammering effect occurs between the rail and the wheel. Conversely, the track exerts an upward pushing force on the rail at the lowest point of vibration. Under the combined action of the wheel and ladder sleeper, the rail is prone to plastic deformation. As the wheel directly contacts the rail, any mismatch in their vibration trends leads to significant interaction and can lead to rail corrugation. In the frequency range of 402–420 Hz, the wheelset primarily undergoes lateral expansion and contraction without significant vertical vibration. This generates substantial lateral forces on the rail, increasing the lateral fastener force. Based on the vibration modes and transfer characteristics at the resonant and anti-resonant frequencies of the wheelset, it is evident that the wheelset's vibration within the range of 0–1000 Hz is much greater than that of the track. The phenomena of vehicle-track resonance and anti-resonance are particularly pronounced in the mid-to-low-frequency range.

The vibration of the vehicle-track system not only affects the generation of rail corrugation but also has a significant impact on the fasteners. To analyze the relationship between the fasteners and vehicle-track vibration, the fastener force receptance was obtained and shown in Fig. 14. It can be observed that the fastener force reaches its peak around 40 Hz, 110 Hz, 404 Hz, 488 Hz, and 75 6Hz. The maximum fastener force occurs around 110 Hz, consistent with the vibration modes of the rail and wheelset. At this frequency, the rail and sleeper exhibit opposite vibration, as shown in Fig. 12. Therefore, at the highest point of rail vibration, the ladder sleeper corresponds to its lowest point, resulting in a peak in fastener force. Although the vibration trend of the ladder sleeper-rail-wheelset is consistent around 756 Hz, the vibration amplitude in the rail is significantly larger than that of the ladder sleeper. This sudden increase in fastener force occurs at this frequency. The rapid fluctuation in long-term operation in fastener force can lead to fatigue failure of the fasteners, especially when the vehicle-track mismatch is present. This phenomenon is in line with severe rail corrugation and fastener failure reported in the literature [22, 23].

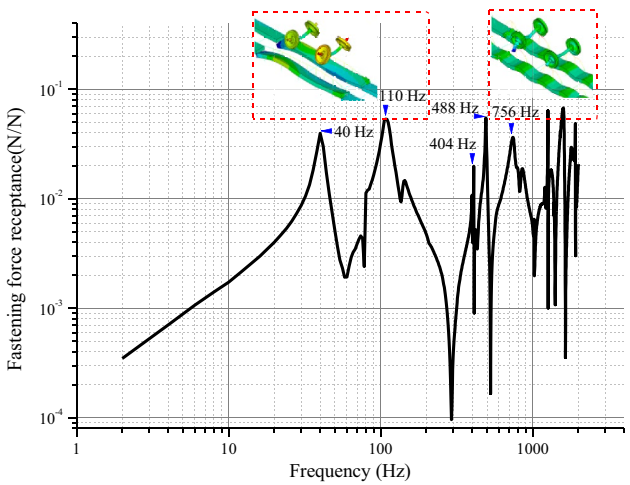

Fig. 14 The receptance of vertical fastening force

Based on the analysis of vibration transmission characteristics for individual wheelsets and tracks, the vertical vibration of the wheel and axle is similar in the range of the first 50 Hz. Within the range of the first 1000 Hz, the wheel experiences more resonances and anti-resonances compared to the axle, resulting in more complex vibration modes. At specific frequencies, the vibration mode of the wheelset may exhibit vertical rigid body vibration, M-shaped vibration, W-shaped vibration, or lateral contraction vibration. Compared with the conventional monolithic track, the influence of the ladder track on the vertical vibration of the rail is mainly concentrated in the range of the first 200 Hz, with less significant influence beyond 200 Hz. In terms of the vibration transmission characteristic analysis for the vehicle-ladder track system, the wheelset experiences significantly greater vibration compared to the ladder track within the first 1000 Hz. Notably, the vehicle-track system shows more pronounced resonance and anti-resonance phenomena within the medium- to low-frequency spectrum. At the frequency of 110 Hz, the motion of the rail is contrary to that of the sleeper, while at 756 Hz, although the motion of the sleeper is the same as that of the rail, the rail's vibration amplitude is much larger than that of the sleeper. Both cases result in an increase in fastening force, and the rapid fluctuation in long-term operation in fastener force can lead to fatigue failure of the fasteners, especially when the vehicle-track mismatch is present.

4 Analysis of the Dynamic Response Characteristics of the Vehicle-Ladder Track Coupling System

To comprehensively investigate the typical dynamic behavior of the vehicle-ladder track-coupled system in actual operating conditions, the system's dynamic performance from a time-domain perspective was examined first. Furthermore, Fourier transform analysis was utilized to compare the variations in characteristic frequencies. Additionally, the impact of typical train running speed on the dynamic response of the system was thoroughly analyzed.

Track irregularities are the main excitation source in urban rail vehicle-track systems and are typically expressed using power spectral density functions [23]. Due to the

relatively late start of research on track irregularity spectra in the urban rail field, there is still a lack of widely accepted standard track irregularity spectra. According to reference [24], the wavelengths of vertical track irregularities in the ladder track are mainly concentrated in the range of 1 to 80 m. Considering the fixed wavelength of track irregularities due to the length of the ladder track and relevant studies on subway track spectra [24, 25], a random track irregularity spectrum is constructed, serving as the input excitation, as shown in Fig. 15.

Figure 16 shows the dynamic response curve of the vehicle-track system at a speed of 36 km/h in the time domain and frequency domain. The sleeper exhibits significant vibration within specific frequency ranges: 72–107 Hz (with a peak at 78 Hz), 130–150 Hz (with a peak at 134 Hz), 273–300 Hz (with a peak at 286 Hz), 350–450 Hz (with peaks at 380 Hz and 430 Hz), 540–635 Hz (with peaks at 578 Hz and 625 Hz), 665–745 Hz (with peaks at 695 Hz and 735 Hz), and 770–790 Hz (with a peak at 780 Hz). The rail exhibits significant vibrations within the following frequency ranges: 405–470 Hz (with peaks at 420 Hz and 432 Hz), 530–650 Hz (with a peak at 575 Hz), 600–680 Hz (with a peak at 666 Hz), 690–755 Hz (with peaks at 698 Hz and 730 Hz), and 770–820 Hz (with peaks at 782 Hz and 796 Hz). The wheel experiences vibrations at peaks near 274 Hz, 440 Hz, and 576 Hz, with its dominant vibrations occurring after 730 Hz. The vibrations of the axle end are concentrated in the following frequency ranges: around 78 Hz, 275 Hz, 358 Hz, 440 Hz, 578 Hz, 780 Hz, and 890 Hz. The vibrations at the axle midpoint are larger than those at the axle end at peaks near 78 Hz, 358 Hz, and 890 Hz, while at other main frequency peaks, the vibrations at the axle end are larger than that at the axle midpoint.

Figure 17 shows the vibration deformation of the vehicle-track system at the moment of maximum acceleration with an excitation speed of 36 km/h. In actual operation, the vibration deformation of the vehicle-track system exhibits similarities to the vibration modes observed in the vibration transmission characteristics of the vehicle-track system. However, there may be slight differences due to the simultaneous excitation of the system by multiple frequency loads. Therefore, the vibration deformation of the vehicle-track system at each moment is a combination of vibration modes at different frequencies, with the combined deformation resembling the vibration modes corresponding to the frequency ranges.

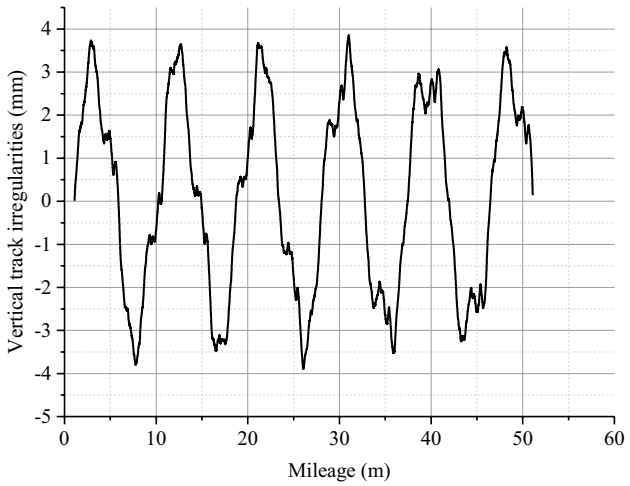

Fig. 15 Generated random track irregularities

The influence of different speeds on the vibration characteristics of the vehicle-track system was also considered by exciting the vehicle-track coupled model at speeds of 36 km/h, 45 km/h, 60 km/h, and 72 km/h. This offers valuable insights into the system's response to various operational conditions and aids in identifying critical areas susceptible to vibration-related issues. The vibration frequency domain of the sleeper, rail, wheel, and axle were compared, as shown in Figs. 18, 19, 20, 21, 22.

From Figure 18, it can be observed that changing the running speed has negligible influence on the dominant resonance frequencies of the sleeper within the first 500 Hz. However, the vibration peaks increase with the speed, reaching maximum values around 78 Hz. The vibration transmission characteristics analysis in 3.3 indicates that 78 Hz corresponds to the anti-resonance frequency of the wheelset and the rail/sleeper, and the vibration peaks also increase with the speed. The vertical vibration accelerations at different speeds all exhibit peaks in the range of 130–140 Hz, with similar vibration amplitudes. This suggests that controlling the running speed has little effect on controlling the vibration of the sleeper at this frequency range. Between 500 Hz and 850 Hz, the dominant vibration frequency range shows significant changes with varying speed. Increasing speed results in larger dominant vibration frequencies (except for a peak near 534 Hz at 72 km/h), but the effect of running speed on vibration peaks is not significant. Therefore, the running speed mainly affects the vibration peaks at the dominant frequencies within the range of the first 500 Hz for the ladder sleeper, while it affects the dominant vibration frequency range beyond 500 Hz.

Figure 19 reveals that with increasing speed, the dominant vibration frequency range of the rail expands, but the vibration peaks show no significant changes with the increase in running speed. Therefore, for the ladder track, controlling the speed to regulate the vibration of the rail has an insignificant effect. These findings correspond with the results documented in the reference [26].

Figure 20 illustrates that within the first 400 Hz, the dominant vibration frequency of the wheel occurs between 270 Hz and 280 Hz. In this dominant frequency range, acceleration in the vertical direction of the wheel remains relatively

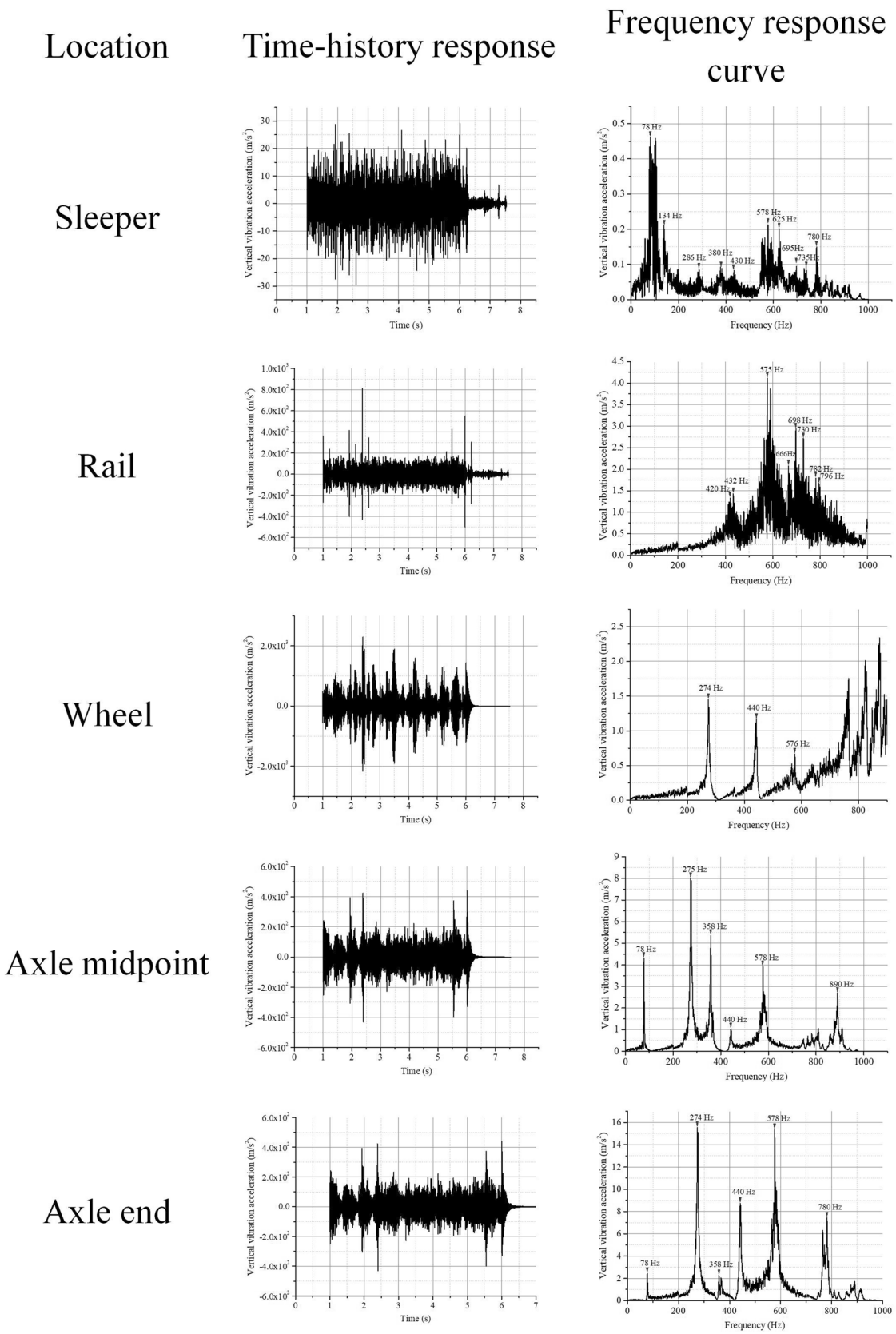

Fig. 16 Dynamic response of the wheel/track at a speed of 36km/h

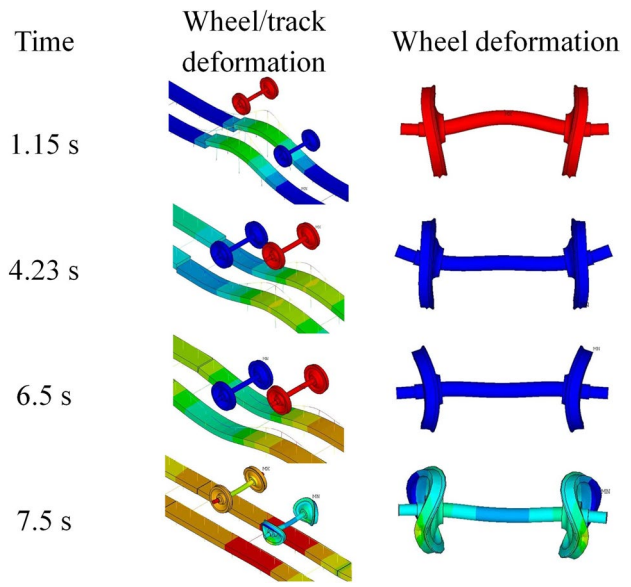

Fig. 17 Vibration and deformation of the wheel/track at different instants of time at a speed of 36km/h

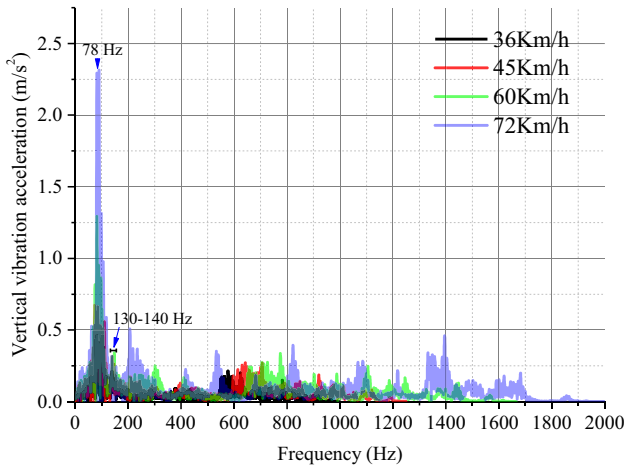

Fig. 18 Comparison of vertical vibration acceleration at the sleeper location for different speeds in the frequency domain

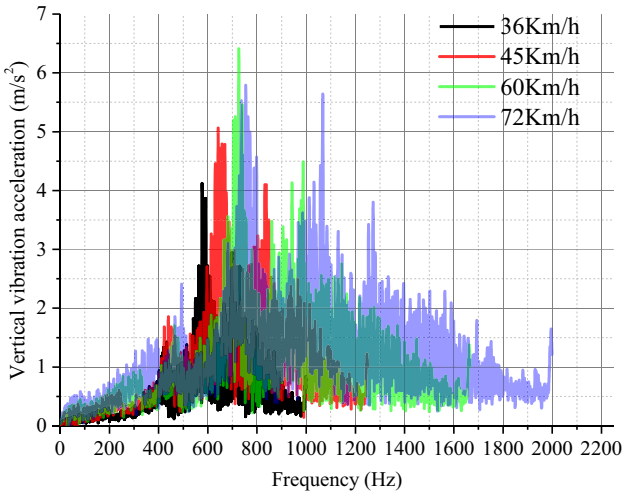

Fig. 19 Comparison of vertical vibration acceleration at the rail location for different speeds in the frequency domain

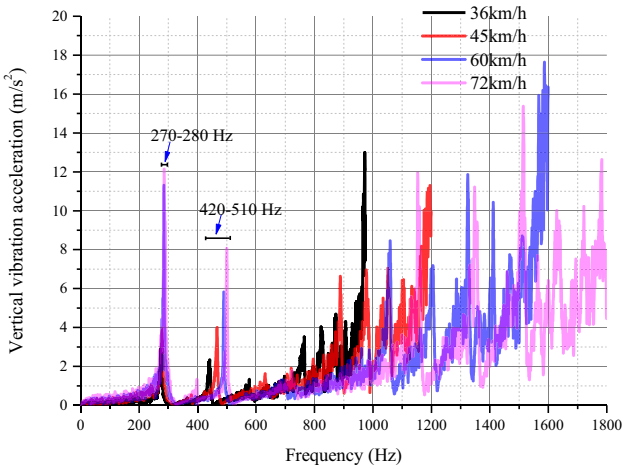

Fig. 20 Comparison of vertical vibration acceleration at the wheel location for different speeds in the frequency domain

unchanged with the increase in running speed. However, the vibration peaks at other dominant frequency ranges increase as the speed increases. Between 420 Hz and 510 Hz, both the dominant vibration frequency and its peak value increase with the speed. Overall, within the first 800 Hz, the vibration primarily occurs between 270 Hz and 280 Hz and between 420 Hz and 510 Hz.

According to Fig. 21, at different speeds, the axle midpoint consistently exhibits vibration peaks around 78 Hz, and these peaks increase in magnitude with the increase in speed. Between 200 Hz and 400 Hz, the dominant vibration frequency does not show significant changes with speed, but the vibration peaks increase as the speed increases. Beyond 400 Hz, the dominant vibration frequency increases with speed, but the vibration peaks do not show significant changes with the increase in speed.

According to Fig. 22, within the first 300 Hz, the dominant vibration frequencies of the axle end occur around 78 Hz and 284 Hz. Apart from the increasing vibration peaks with speed, the vibration frequencies do not show significant changes with speed. Beyond 300 Hz, the dominant vibration frequencies of the axle end increase with speed, but the vibration peaks do not show significant changes with speed.

The comparison of maximum vertical vibration accelerations (MVVA) at different positions and speeds is presented in Fig. 23. It can be observed that MVVA for both the track

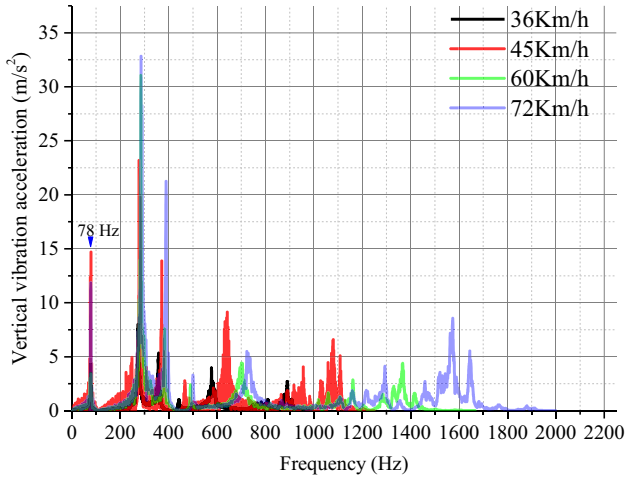

Fig. 21 Comparison of vertical vibration acceleration at the axle midpoint for different speeds in the frequency domain

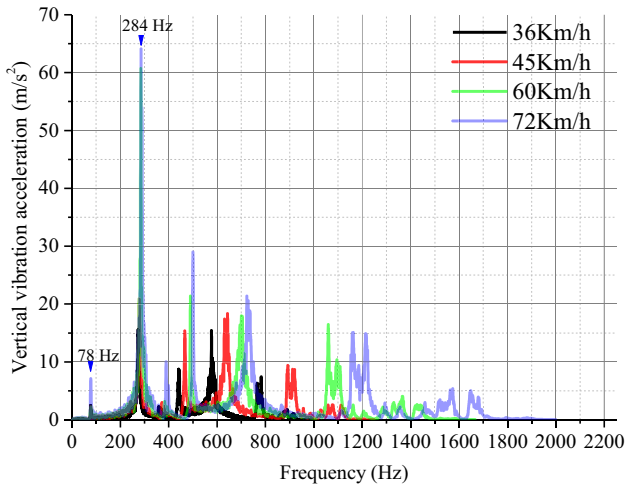

Fig. 22 Comparison of vertical vibration acceleration at the axle end for different speeds in the frequency domain

and wheelset increases with speed. Specifically, the MVVA at the wheel and axle end is higher than that at the axle midpoint, rail, and sleeper, while the MVVA at the sleeper is the lowest, and the axle midpoint exhibits an MVVA nearly identical to that of the rail. Moreover, as the speed increases, the relative rates of increase in MVVA compared to that at 36 km/h are depicted in Fig. 23. It can be observed that the axle end and wheel exhibit the highest rate of increase, followed by the axle midpoint, rail, and sleepers.

5 Conclusions

This study established a three-dimensional flexible FE model of the vehicle-ladder track system, investigating

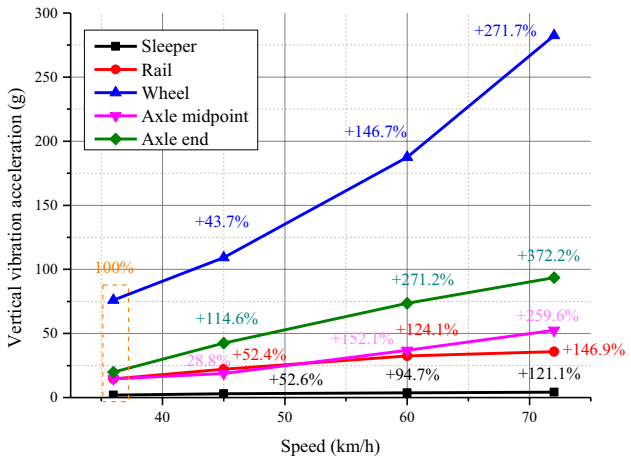

Fig. 23 Comparison of the maximum vertical vibration acceleration at different locations for different speeds

thorough vibration transmission characteristics and dynamic responses crucial for implementing effective mitigation strategies. Based on the analysis, the following conclusions were derived:

1. The wheelset-track resonance and anti-resonance phenomena were more prominent in the medium- to low-frequency range. At specific frequencies, the wheelset exhibited various vibration modes, including vertical rigid body vibration, M-shaped vibration, W-shaped vibration, and lateral contraction vibration. In conjunction with the vibration modes of the wheelset-ladder system, an increase in fastening force could occur due to the relatively substantial vibrations of the rail and ladder sleeper, whether they were in opposing directions or in the same direction with significant amplitudes. This observation aligned with the documented instances of severe rail corrugation and fastener failures in the existing literature.
2. The research of the dynamic response of the coupled system revealed that the speed primarily affected (***a***) the vibration peak values below 500 Hz and the dominant frequency range beyond 500 Hz for the sleeper; (***b***) the dominant vibration frequency range of the rail; (***c***) the vibration peak values at the dominant vibration frequencies below 400 Hz for the wheel (except for 270–280 Hz), the dominant vibration frequency range and peak values within 420–510 Hz; (***d***) the vibration peak values within 400 Hz and the dominant vibration frequency beyond 400 Hz for axle midpoint; and (***e***) the dominant vibration frequencies after 300 Hz for the axle end.
3. The maximum vertical vibration acceleration of both the track and wheelset increased with speed, with the wheel experiencing the largest acceleration, the sleeper the lowest, and the axle midpoint almost identical to the

rail. In terms of the increased rate of maximum vibration acceleration, the axle end and the wheel exhibited the highest rate of increase, followed by the axle midpoint, rail, and sleepers.

4. Although this study provides a comprehensive model to simulate the dynamic behavior of vehicle-ladder track systems, it does not address specific field-applicablecontrol measures for mitigating observed damage. Therefore future research should develop practical strategies to address these issues.

Acknowledgements This work was supported by the National Key R&D Program, grant number 2021YFB2600600 2021YFB2600601, and the Natural Science Basic Research Plan in Shaanxi Province of China grant number 2022JQ-483 and the China Postdoctoral Science Foundation grant number 2022M720533.

Declarations

Conflict of interest The authors declare no conflict of interest.

References

1. Hosking RJ and Milinazzo F (2012) Modelling the floating ladder track response to a moving load by an infinite Bernoulli-Euler beam on periodic flexible supports: East Asian Journal on Applied Mathematics 2(4):285–308
2. Deng YS, Xia H, Zenda Y, Inoue H, and Qi L (2011) Experimental study of ladder track on a rail transit elevated bridge: Engineering Mechanics 28(3):49–054
3. Xia H, Chen J, Xia C, Inoue H, Zenda Y, and Qi L (2010) An experimental study of train-induced structural and environmental vibrations of a rail transit elevated bridge with ladder tracks: Proceedings of the Institution of Mechanical Engineers, Part F: Journal of Rail and Rapid Transit 224(3):115–124
4. Xia H, Deng Ys, Zou Yw, De Roeck G, and Degrande G (2009) Dynamic analysis of rail transit elevated bridge with ladder track: Frontiers of architecture and civil engineering in china 3:2–8
5. Wakui H (1997) Ladder sleepers perform well in tests: Railway Gazette International:589–592
6. Yan ZQ, Gu AJ, Liu WN, Markine V, and Liang QH (2012) Effects of wheelset vibration on initiation and evolution of rail short-pitch corrugation: Journal of Central South University 19(9):2681–2688
7. Li W, Wang HY, Wen ZF, Du X, Wu L, Li X, and Jin XS (2016) An investigation into the mechanism of metro rail corrugation using experimental and theoretical methods: Proceedings of the Institution of Mechanical Engineers, Part F: Journal of Rail and Rapid Transit 230(4):1025–1039
8. Wang P, Lu J, Zhao CY, Chen MM, and Xing MT (2021) Numerical investigation of the fatigue performance of elastic rail clips considering rail corrugation and dynamic axle load: Proceedings of the Institution of Mechanical Engineers, Part F: Journal of Rail and Rapid Transit 235(3):339–352
9. Liu WN, Ren J, Liu WF, Wang WB, and Zhang HG (2011) In-situ tests and analysis on rail corrugation of Beijing Metro: Urban Rapid Rail Transit 24(3):6–9
10. Grassie S (2009) Rail corrugation: characteristics, causes, and treatments: Proceedings of the Institution of Mechanical Engineers, Part F: Journal of Rail and Rapid Transit 223(6):581–596
11. Xiao H, Yang S, Wang HY, and Wu SX (2018) Initiation and development of rail corrugation based on track vibration in metro systems: Proceedings of the Institution of Mechanical Engineers, Part F: Journal of Rail and Rapid Transit 232(9):2228–2243
12. Li X, Ren Z and Wang Z (2020) Study on rail corrugation of ladder-type sleeper track based on vibration characteristics: J China Railway Soc 42(10):38–44
13. Li X, Li W, Shen Y, Wen Z, and Jin X (2016) Study on the rail corrugation of the ladder-type sleepers track based on the track vibration theory: Journal of Mechanical Engineering 52(22):121–128
14. Fan Q, Jiang W and Cai C (2021) Dynamic performance analysis of trapezoidal sleeper track of metro train running with high speed: Railway Enginnering 61(01):114–118
15. Jin H, Liu WN and Wang WB (2013) Analysis of modal test of the ladder track: Engineering Mechanics 30(03):459–463
16. Yan ZQ, Markine V, Gu AJ, and Liang QH (2014) Optimisation of the dynamic properties of ladder track to minimise the chance of rail corrugation: Proceedings of the Institution of Mechanical Engineers, Part F: Journal of Rail and Rapid Transit 228(3):285–297
17. Wang YK, He ZX, Feng QB, Su C, Wang X, Bao NN, Wang HY, Yun JF, and Bai YB (2022) Influence of vibration suppression device for ladder-type sleeper track on vehicle-track system dynamic interaction: Yanbo, Influence of Vibration Suppression Device for Ladder-Type Sleeper Track on Vehicle-Track System Dynamic Interaction
18. Jin H, Liu WN and Zhou SH (2015) Optimization of vibration reduction ability of ladder tracks by FEM coupled with ACO: Shock and Vibration 2015
19. Jin H and Liu W (2012) Vibration reduction optimization of ladder track based on an ant colony algorithm: Journal of Central South University (Science and Technology) 43(7):2751–2756
20. Yan Z, Markine V, Gu A, and Liang Q (2014) Optimisation of the dynamic properties of ladder track to minimise the chance of rail corrugation: Proceedings of the Institution of Mechanical Engineers, Part F: Journal of Rail and Rapid Transit 228(3):285–297
21. Yan ZQ, Markine V, Gu AJ, and Liang QH (2014) Optimization of the dynamic properties of the ladder track system to control rail vibration using the multipoint approximation method: Journal of Vibration and Control 20(13):1967–1984
22. Mohammadzadeh S and Mehrali M (2017) Dynamic response of ladder track rested on stochastic foundation under oscillating moving load: Journal of Theoretical and Applied Mechanics 55(1):281–291
23. Hei Y (2019) Analysis and treatment of fastener defects caused by metro rail corrugation: Railway Engineering 59(8):150–153

24. Yang HX, Sun X and Zhang HG (2012) Features and treatment measures for unusual rail corrugations in urban rail transit: Urban Rapid Rail Transit 25(5):105–108
25. Lu W, Ma S, Gao L, and Liu X (2020) Analysis of Track Irregularity Spectrum of the Beijing Subway Lines: Journal of Railway Engineering Society 37(03)
26. He YL, Li Zw, Sheng CL, and Chen X (2014) Characteristic analysis of track spectrums of different subway line conditions: Journal of Railway Engineering Society 8:99–104
27. Yan ZQ. Optimization study of the dynamic properties of ladder track to minimize the probability of rail corrugation. 2014, Beijing Jiaotong University